ADVANCED FUNCTIONAL MATERIALS
www.afm-journal.de

An Intrinsically Stretchable High-Performance Polymer Semiconductor with Low Crystallinity

Yu Zheng, Ging-Ji Nathan Wang, Jiheong Kang, Mark Nikolka, Hung-Chin Wu, Helen Tran, Song Zhang, Hongping Yan, Hu Chen, Pak Yan Yuen, Jaewan Mun, Reinhold H. Dauskardt, Iain McCulloch, Jeffrey B.-H. Tok, Xiaodan Gu, and Zhenan Bao**

For wearable and implantable electronics applications, developing intrinsically stretchable polymer semiconductor is advantageous, especially in the manufacturing of large-area and high-density devices. A major challenge is to simultaneously achieve good electrical and mechanical properties for these semiconductor devices. While crystalline domains are generally needed to achieve high mobility, amorphous domains are necessary to impart stretchability. Recent progresses in the design of high-performance donor–acceptor polymers that exhibit low degrees of energetic disorder, while having a high fraction of amorphous domains, appear promising for polymer semiconductors. Here, a low crystalline, i.e., near-amorphous, indacenodithiophene-*co*-benzothiadiazole (IDTBT) polymer and a semicrystalline thieno[3,2-*b*]thiophene-diketopyrrolopyrrole (DPPTT) are compared, for mechanical properties and electrical performance under strain. It is observed that IDTBT is able to achieve both a high modulus and high fracture strain, and to preserve electrical functionality under high strain. Next, fully stretchable transistors are fabricated using the IDTBT polymer and observed mobility ≈0.6 $cm^2 V^{-1} s^{-1}$ at 100% strain along stretching direction. In addition, the morphological evolution of the stretched IDTBT films is investigated by polarized UV–vis and grazing-incidence X-ray diffraction to elucidate the molecular origins of high ductility. In summary, the near-amorphous IDTBT polymer signifies a promising direction regarding molecular design principles toward intrinsically stretchable high-performance polymer semiconductor.

1. Introduction

Stretchable and conformable electronic devices have recently gathered much interests for their potential in enabling advanced wearable,[1,2] implantable,[3] and health monitoring applications,[4–6] ranging from robotic sensory skins,[7] wearable communication devices[8,9] to biocompatible integrated circuits.[10] Currently, stretchable electronics has been achieved using geometric approaches such as strain engineering,[11] induced buckling,[12] and Kirigami interconnects on rigid silicon-based devices.[13] However, to achieve low-cost, large-area, and high-density device manufacture, next-generation wearable and implantable electronic devices could greatly benefit from intrinsically stretchable materials. Transistors are basic elements for processing information and simple logic operations.[14,15] To enable fully stretchable transistors, each component in the device, including stretchable dielectrics,[16,17] substrates,[18] and conductors,[19–21] has been developed. However, a major challenge remains in the design of stretchable semiconductor material that maintains good electronic properties under mechanical strain.[22]

The field of intrinsically stretchable polymer semiconductor has witnessed significant growth in recent years.[23] Various structural modification strategies have been reported, such as backbone engineering[24,25] and side-chain engineering,[26,27] which include flexible conjugation breakers,[28] longer and softer side chain,[29] or tuning the size and number of electron-donating thiophene groups.[30]

Y. Zheng, Dr. G.-J. N. Wang, Dr. J. Kang, Dr. M. Nikolka, Dr. H.-C. Wu, Dr. H. Tran, Dr. H. Yan, J. Mun, Dr. J. B.-H. Tok, Prof. Z. Bao
Department of Chemical Engineering
Stanford University
Stanford, CA 94305-5025, USA
E-mail: zbao@stanford.edu

S. Zhang, Prof. X. Gu
School of Polymer Science and Engineering
The University of Southern Mississippi
Hattiesburg, MS 39406, USA
E-mail: xiaodan.gu@usm.edu

The ORCID identification number(s) for the author(s) of this article can be found under https://doi.org/10.1002/adfm.201905340.

Dr. H. Chen, Prof. I. McCulloch
King Abdullah University of Science and Technology (KAUST)
Kaust Solar Center (KSC)
Thuwal 23955-6900, Saudi Arabia

Dr. P. Y. Yuen
Department of Mechanical Engineering
Stanford University
Stanford, CA 94305, USA

Prof. R. H. Dauskardt
Department of Materials Science & Engineering
Stanford University
Stanford, CA 94305, USA

DOI: 10.1002/adfm.201905340

The general design principle is to decrease the overall crystallinity of the polymer film while maintaining good electrical connections between aggregates, thus maintaining good charge transport. When a strain is applied, the amorphous region is more easily stretched through polymer conformation change to dissipate the strain energy, making the polymer film ductile and stretchable.[31] However, it remains challenging to maintain good charge transport properties while having mechanical compliance. This is due to the decreased π–π stacking between neighbor polymer chains when the overall crystallinity is decreased, resulting in reduced interchain transport efficiency across the film within these semicrystalline systems.[32] Other approaches, such as cross-linking[33] and nanoconfinement,[34] typically require fine tuning of processing conditions which may have a large number of parameter space to screen.

Recent reports have indicated that highly crystalline morphology may not be necessary for polymer semiconductor to have high charge carrier mobilities.[35–37] Instead, short-range intermolecular aggregation combined with efficient intramolecular charge transport was sufficient for good long-range charge transport, and the limiting step was "trapping" caused by energetic disorder. There has been much progress recently in designing donor-acceptor conjugated polymers that exhibit high charge carrier mobilities despite possessing near-amorphous morphology.[38,39] Herein, we investigate the potential of a conjugated polymer indacenodithiophene-*co*-benzothiadiazole (IDTBT) previously reported as "near-amorphous" as an intrinsically stretchable polymer semiconductor candidate. Indeed, despite its low crystallinity in a thin film, it exhibits high charge carrier mobility of 1.5–2.5 $cm^2\ V^{-1}\ s^{-1}$ and near-ideal transistor current–voltage behavior.[40] We hypothesize that the lack of long range order and high fraction of amorphous regions may allow the IDTBT polymer chains to slide past each other or become stretched under strain, resulting in mechanisms for strain energy dissipation. Thus, high charge carrier mobility and high stretchability may be achieved simultaneously in one polymer system. In addition, IDTBT exhibits good air-stability,[41] which is important for operational shelf life stability of devices. Its high solubility in a wide range of solvents makes this polymer promising for plastic electronics.

Most studies on indacenodithiophene-based (IDT-based) donor–acceptor copolymer focused on its charge transport properties instead of its mechanical properties.[42] Luscombe and coauthors studied a series of alkyl-IDT polymers with different degrees of backbone twists,[43] and the elastic modulus and crack-on-set strain were measured by film-on-elastomer method. However, there is no systematic comparison study between the near-amorphous and semicrystalline conjugated polymer system, in terms of electrical and mechanical properties. In addition, no stretchable devices have been fabricated to characterize IDTBT in a final device and its potential for stretchable electronics. In this study, we chose IDTBT as a model compound to investigate the molecular design guidelines for next-generation intrinsically stretchable high-performance conjugated polymer, and with the semicrystalline thieno[3,2-b]thiophene-diketopyrrolopyrrole (DPPTT) being employed as a comparison. We chose diketopyrrolopyrrole (DPP)-based polymer as comparison because it is a common donor-acceptor system reported to possess high charge transport properties.[44] Also, its strong intermolecular interactions have led to ordered microstructures with closely packed crystalline domains. In addition, DPP served as the building block for many developed intrinsically stretchable polymer semiconductors.[33,34,45]

As stated earlier, the unique near-amorphous morphology of IDTBT would make it potentially stretchable, while the rigid backbone configuration would maintain its charge transport under strain. Our performed mechanical characterizations indicated that IDTBT does not follow the typical trend for most conjugated polymers because high modulus and high stretchability can be achieved simultaneously in this low-crystallinity system, which is different with the reported summarized relationship between modulus and stretchability of most donor-acceptor polymer.[30] Next, we proceeded to fabricate high-performance fully stretchable transistors with IDTBT as the polymer semiconductor to demonstrate that IDTBT has sufficiently good electrical properties under mechanical strain. Without strain, the devices showed ideal transfer characteristics with high mobility around 1.8 $cm^2\ V^{-1}\ s^{-1}$. The mobility remained stable at ≈0.6 $cm^2\ V^{-1}\ s^{-1}$ at 100% strain along stretching direction, compared to the rapidly decreasing of charge carrier mobility to 5×10^{-4} $cm^2\ V^{-1}\ s^{-1}$ for the semicrystalline DPPTT-based stretchable transistors. Furthermore, morphology investigation of stretched IDTBT films was carried out to show that the high stretchability originates from sliding and alignment of polymer chains, which can dissipate strain energy. The deformation modes for these two polymer films were different under strain (**Figure 1**), in which IDTBT showed higher stretchability while DPPTT was brittle. When the strain was released, in contrast to the crack size changes for DPPTT, wrinkles were formed for IDTBT film.

2. Results and Discussion

2.1. Mechanical Characterizations

According to our grazing-incidence X-ray diffraction (GIXD) results for spin-coated IDTBT and DPPTT films to be discussed in more details (Figure 4b), IDTBT showed face-on orientation and diffracted weakly, with broad and diffuse (010) peak (originated from π–π stacking diffraction) in the out-of-plane direction. In contrast, 2D GIXD images for DPPTT showed an edge-on orientation and strong diffractions of (h00) lamella peaks up to the fourth-order. This is consistent with earlier results that IDTBT has a near-amorphous microstructure[42] while DPPTT has a semicrystalline microstructure.[44] It has been reported that molecular weight of polymer strongly influences the degree of stretchability of semiconducting polymer thin films.[46,47] Therefore, we investigated IDTBT and DPPTT with comparable number average molecular weights M_n (108.6 and 80.1 kg mol^{-1}, respectively) and dispersities (**Table 1**).

To study the impact of having nearly amorphous microstructure on thin film mechanical properties, pseudo free-standing tensile tests on the IDTBT and DPPTT were performed.[30,48] The experimental set up involves floating polymer thin films on water for stress–strain characterizations. This "film-on-water" technique[49] decouples the effects from substrates thus allowing a more accurate measurement of the bulk polymer

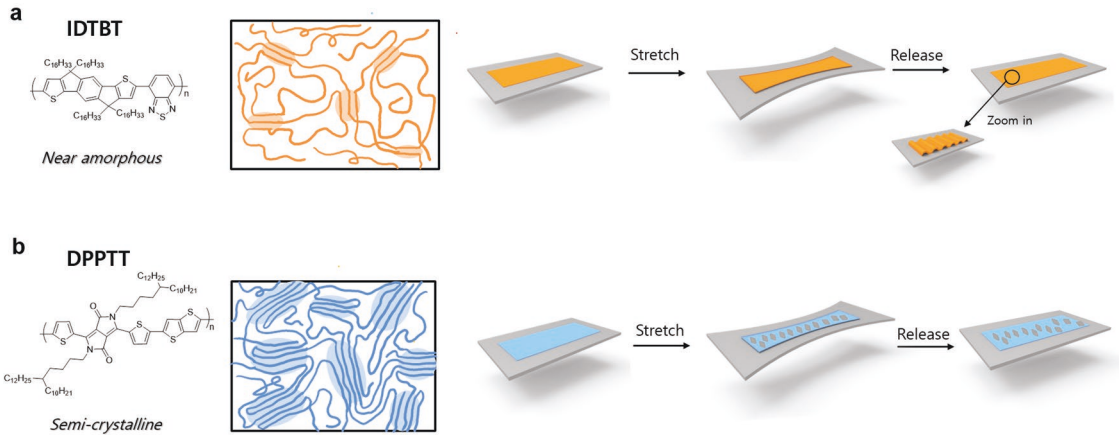

Figure 1. Schematic illustrating the different mechanical deformation modes for semiconducting polymer thin films with different morphology: a) IDTBT; b) DPPTT.

film (typically microthick) mechanical properties, as compared to the traditional buckling method[50] and crack-on-set strain methods.[51] The latter two have been applied to thin polymer films (<1 µm thickness). The average elastic modulus and fracture strain are summarized in Table 1. Notably, the stress–strain curve shows that IDTBT possesses a higher elastic modulus and higher fracture strain than DPPTT (**Figure 2**a). An averaged elastic modulus of 745 ± 90 MPa and fracture strain of 22 ± 1.1% were observed for IDTBT, whereas an averaged elastic modulus of 374 ± 25 MPa and fracture strain of 9 ± 3.3% were observed for DPPTT. This contradicted the typical observations that higher crystallinity usually correspondingly gives a higher modulus and lower stretchability.[52] IDTBT lacks long range π-π stacking, yet its modulus is still higher than DPPTT with high crystallinity. Based on a previous report, the near-torsion-free backbone conformation of IDTBT is confirmed by pressure-dependent Raman spectroscopy and simulation results. It was concluded that the IDTBT backbone is rigid and coplanar in thin film state. Thus, we infer that the amorphous microstructure of IDTBT resulted in high stretchability, its high modulus was attributed to the rigid backbone configuration.[53] The high modulus of IDTBT was further confirmed with nanoindentation tests, where the elastic modulus was measured at different tip depths into the total film thickness. Consistent with our "film-on-water" results, IDTBT has a higher modulus than DPPTT (Figure 2b). It was previously reported that IDTBT exhibited a low elastic modulus (360 MPa);[43] this is attributed to the lower molecular weight (15 kg mol^{-1}). Furthermore, the stress–strain curve for IDTBT film indicated yielding behavior before fracture. The yielding behavior is a plastic deformation mode under mechanical strain, commonly observed for ductile polymer thin films.[54] It is typically attributed to molecular processes, such as secondary relaxation and flow of polymer chains. In addition, we performed stress relaxation measurements to confirm the plastic deformation and elucidate the difference in viscoelastic properties between IDTBT and DPPTT. We observed that IDTBT indeed relaxed faster than DPPTT, and it can also reach a lower strain plateau after 500 seconds (Figure 2c). This indicates that the energy loss and dissipation via plastic deformation in the IDTBT thin film is faster than in DPPTT.[48] The stress–strain curve of IDTBT was typical for a polymer with high toughness.[55] IDTBT could withstand much more strain energy during stretching before its final failure.

Table 1. Molecular parameters and mechanical properties of semiconducting polymers. Number average molecular weight (M_n), weight average molecular weight (M_w), and dispersity ($Đ$) were measured by high-temperature gel permeation chromatography (HT-GPC).

Polymers	M_n [kg mol^{-1}]	M_w [kg mol^{-1}]	$Đ$	DP[a)]	E[b)] [MPa]	Fracture[c)] strain [%]
IDTBT	108.6	295.4	2.7	81.9	745	22
DPPTT	80.1	243.1	3.0	62.4	374	9

[a)]Degree of polymerization; [b)]Average elastic modulus of polymer thin film measured by film-on-water experiments, as described in the Experimental Section; [c)]Average fracture strain of polymer thin films as determined by film-on-water experiments.

The glass transition temperature (T_g) for a conjugated polymer is another important parameter for gauging the degree of ductility.[56,57] Typically, a lower backbone T_g corresponds to a higher tendency for plastic deformation upon stretching. Dynamic mechanical analysis (DMA) was performed for an IDTBT thin film drop-casted on polyimide substrate. An alkyl side chain T_g of –8.8 °C and a backbone T_g of 70.4 °C were observed respectively (Figure 2d). For the semicrystalline conjugated polymers DPPTT, only the alkyl side chain T_g could be observed by DMA measurement reported in our previous work.[58] The observation of backbone T_g for IDTBT film confirmed the presence of amorphous domains and free volume. This may explain its higher ductility.

The above mechanical characterizations suggest that IDTBT does not follow the typical trend observed for other conjugated polymers. First, a high modulus may not necessarily correspond to a high crystallinity. IDTBT has a high modulus due to its rigid backbone but still possess a low crystallinity. Second, a high modulus may not always give a low stretchability. In the case of IDTBT, it exhibited ductility despite of its high modulus owing to its near-amorphous microstructure. Third, conjugated polymers with fused rings tend to be rigid and brittle.[59] However, IDTBT films did not show brittleness likely due to the

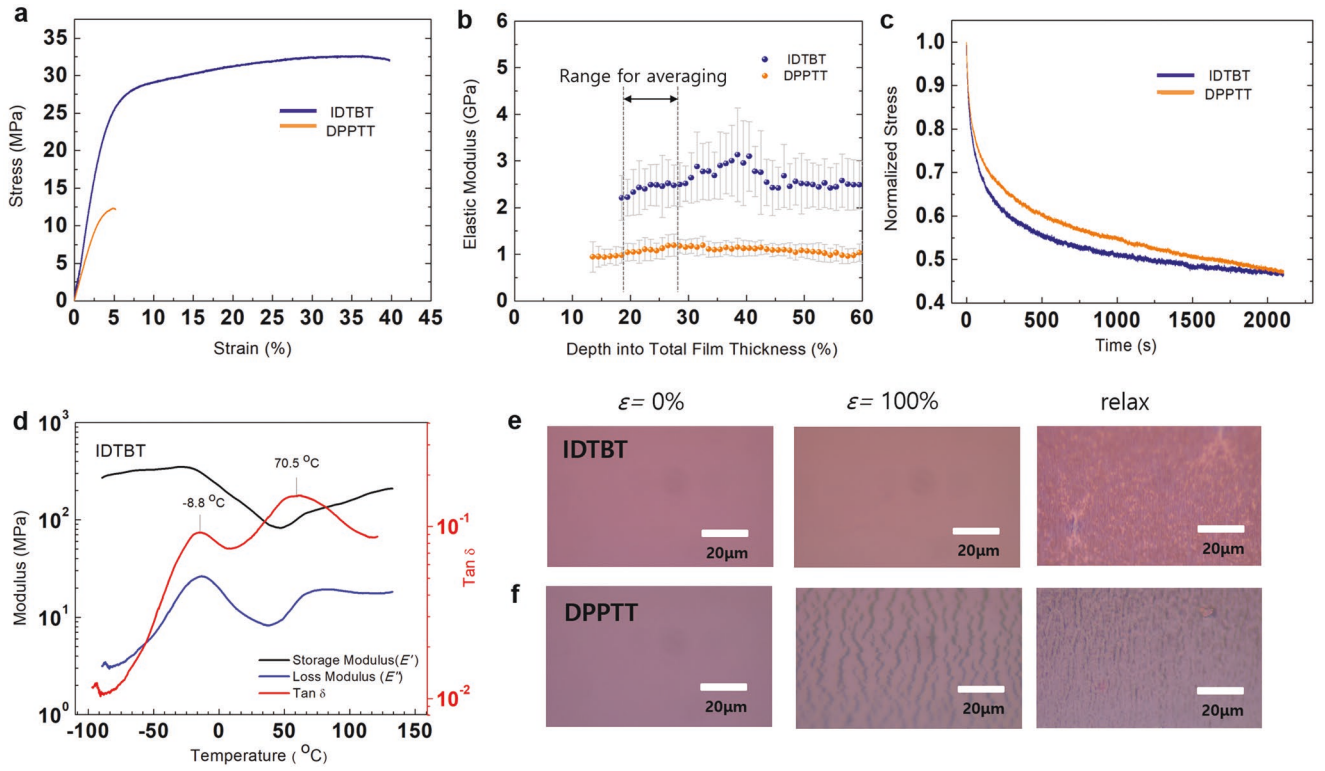

Figure 2. Mechanical property characterizations for polymer thin films. a) The representative stress–strain curves for IDTBT and DPPTT obtained by the film-on-water technique. Thickness of the film: IDTBT 60 nm, DPPTT: 40 nm. b) The elastic modulus at different thin film depths for IDTBT and DPPTT measured by nanoindentation tests. c) Stress-relaxation behavior for polymer thin films upon deformation. Thin films were relaxed from before the fracture strain values. For IDTBT, 20% strain; DPPTT, 5% strain. d) Storage modulus (E'), loss modulus (E''), and tan δ of IDTBT measured by dynamic mechanical analysis (DMA) in the temperature sweep mode. Crack on-set strain measurement for e) IDTBT and f) DPPTT thin films supported by a PDMS substrate. Cracks were monitored by optical microscope from 0% strain to 100% strain.

flexible alkyl side chains configurations that resulted in poor intermolecular packing, which may result in a mechanically weak direction.[60] Hence, IDTBT can serve as an interesting case study to understand critical parameters at the molecular level for the design of stretchable semiconductors.

For stretchable device applications, the polymer semiconductor was deformed on a supported dielectric elastomer. Thus, we examined the crack on-set strain for the polymer thin films on poly(dimethylsiloxane) substrate (PDMS). The polymer films were transferred to PDMS, stretched, and monitored by optical microscope with increasing strain[61] (Figure 2e,f). For DPPTT, appearance of cracks was initially observed at 50% strain. Both the average crack size and density increased with increasing strain, which is typical fracture behavior of brittle polymer thin films (Figure S1, Supporting Information). In contrast, no cracks were observed for IDTBT until 100% strain. Even at 130% strain, only diamond-shaped microvoids were observed, which is a typical fracture behavior of ductile polymer thin films.[62] (Figure S1, Supporting Information). In addition, we performed SEM (Scanning Electron Microscope) for stretched IDTBT and DPPTT films (Figure S20, Supporting Information). At 100% strain, there is no crack formation for IDTBT, while for DPPTT, the cracks could be clearly observed. These results further confirmed the higher ductility of IDTBT thin films. IDTBT films that were stretched then released showed apparent wrinkles, whereas DPPTT films that were stretched then released showed closed cracks. In summary, these crack-on-set measurements confirmed the polymer semiconductors with different morphologies would fracture in different ways on supported dielectric elastomer. Without crack formation even at 100% strain, IDTBT is a promising candidate for stretchable electronics application.

2.2. Morphological Characterizations

Since the macroscopic characterizations of IDTBT thin films suggested promising mechanical properties, we investigated morphological evolution of IDTBT thin film under strain, using both UV–vis absorption and GIXD, to understand the interplay between mechanical and electrical properties. First, we studied the UV–vis absorption (Figure S2, Supporting Information) for IDTBT thin films at different strains and polarization to calculate the dichroic ratio, the absorption ratio of the thin film with polarized light parallel and perpendicular to strain direction (**Figure 3**a). For IDTBT, the dichroic ratio increased linearly with applied strain, which correlates to a steady increase in polymer chain alignment along the strain direction[63] and absence of crack formation (Figure 3b). In contrast, for DPPTT, the dichroic ratio did not increase linearly with applied strain after 25% strain, which correlated to crack formations (Figure 3b). Moreover, polymer chain alignment for IDTBT film was further

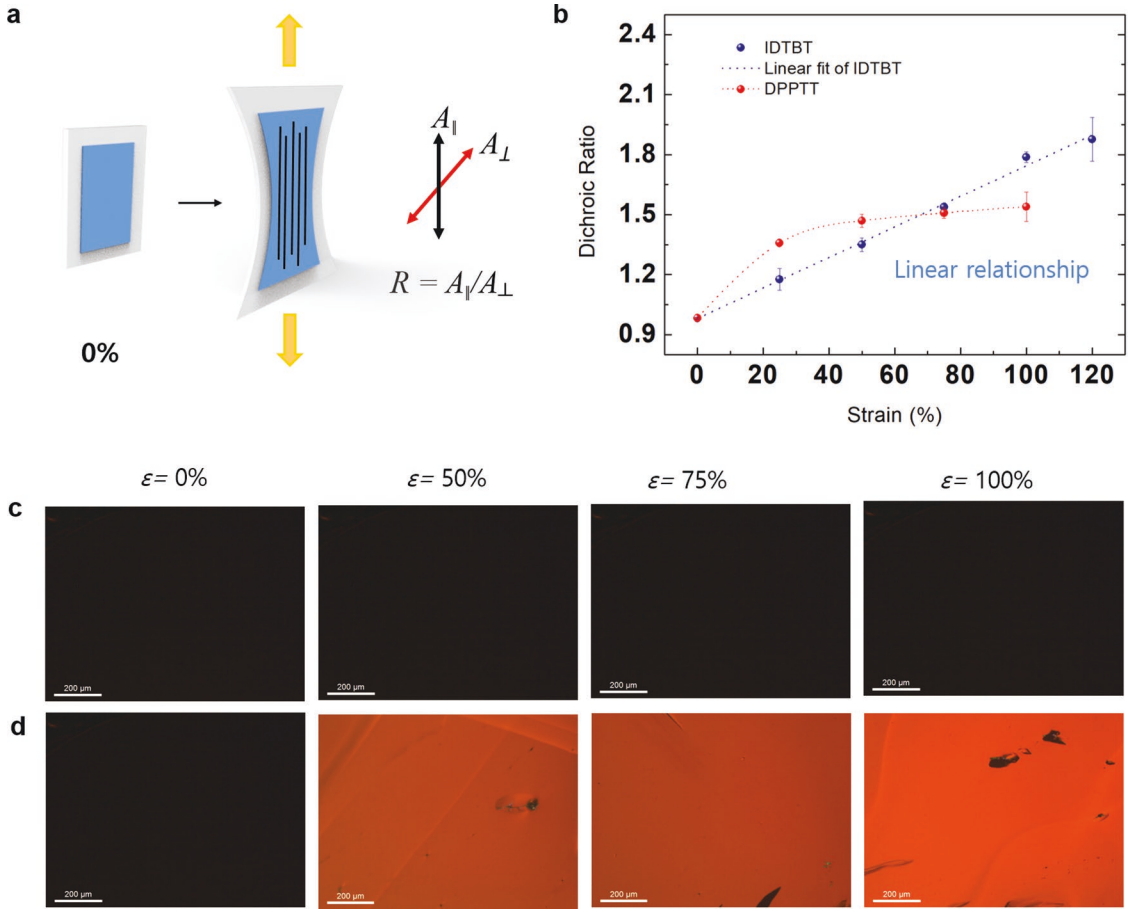

Figure 3. Morphology characterization for IDTBT thin films with optical spectroscopic methods. a) The experiment set-up for dichroic ratio measurement. b) The change of dichroic ratio with increasing applied strain for IDTBT film. The absorption of PDMS substrate was corrected. Polarized microscope measurement for IDTBT film at different strain. The polarizer and analyzer were set perpendicular to each other: c) without sample rotation; d) with sample rotated by 45°.

confirmed by polarized light microscopy (Figure 3c,d). Without applied strain, the film was isotropic, regardless of sample rotation. However, when strain was applied, the IDTBT film displayed prominent anisotropic light transmission, indicating polymer chain alignment. For DPPTT, due to crack formation, the anisotropic light transmission is not as obvious as IDTBT during stretching (Figure S3, Supporting Information).

Next, morphological changes in IDTBT thin films under strain were further investigated using Grazing-incidence X-ray diffraction (GIXD). Compared to the UV–vis spectroscopy, GIXD is able to analyze orientation of crystalline domain, degree of crystallinity, and π-π stacking distance. Basically, IDTBT films were stretched by supporting them on PDMS with different strain levels, and then transferred back to Si substrates for GIXD measurement. We confirmed that there was no relaxation of the strained polymer chains during and after transferring by confirming that the dichroic ratio was unchanged (Figure S4, Supporting Information). **Figure 4**a shows a schematic with the GIXD X-ray beam in different direction relative to stretched IDTBT films. The 2D diffraction patterns (Figure 4b) of pristine IDTBT film (0% strain) resembled the earlier studies of this polymer.[38,42] The broad and diffused peak in the out-of-plane direction indicated that crystallinity of IDTBT was low and the stacking orientation was poor. This was characterized as a "near amorphous" morphology for IDTBT films in previous reports.[38,40] In addition, a (010) peak (i.e., π–π stacking) at q_z direction of 1.55 Å^{-1} was observed, and a π-π stacking distance of 4.1 Å was calculated by Bragg equation ($d = 2\pi/q$). This π–π spacing is much larger than the usual high mobility conjugated polymers (e.g., 3.6 Å of DPPTT),[64] suggesting the large free volume of IDTBT backbone may be originated from the loose molecular packing and disorders observation of out-of-plane π–π stacking. This suggests that the small fraction of crystalline IDTBT took face-on arrangement for the backbone relative to substrate, which may hence facilitate three-dimensional charge transport pathway.[65] On the other hand, the (001) diffraction at $q = 0.41$ Å^{-1}, corresponding to a d-spacing of 15.5 Å, was observed in in-plane direction. It was assigned as the packing distance of repeating units along polymer backbone, which closely matched the theoretical repeat unit length calculation of 16.1 Å.[42] Similar molecular packing feature regarding backbone diffraction signals was observed with conjugated NDI-based polymer system.[66] Such backbone diffraction signal indeed can represent packing structures of IDTBT and, furthermore, described the polymer chain packing anisotropy after stretching.

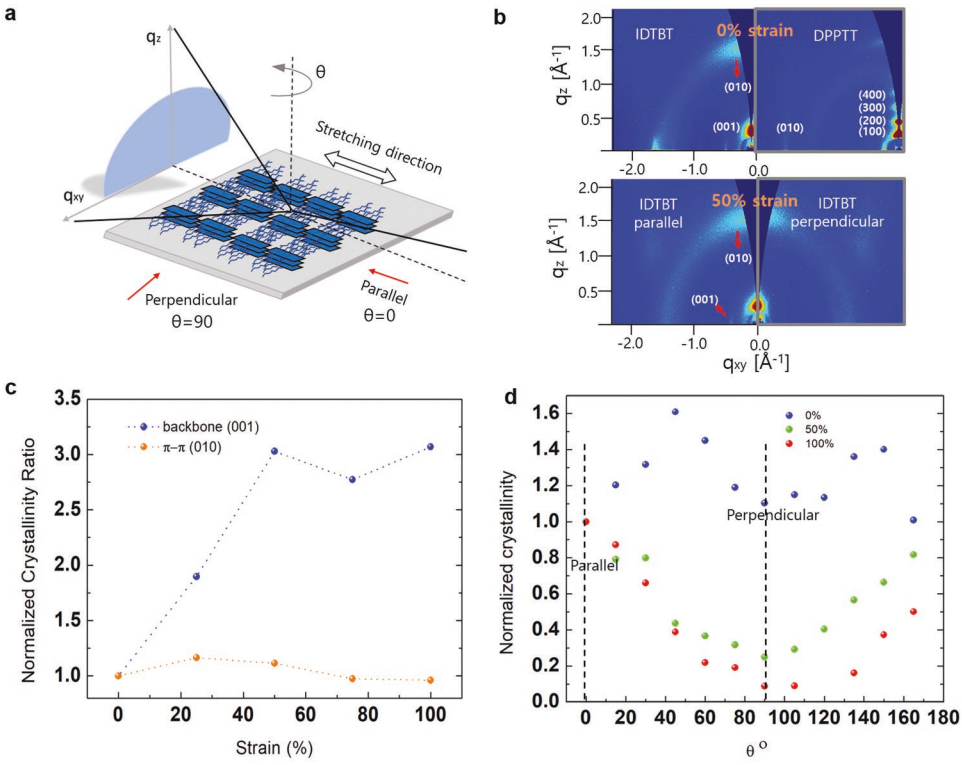

Figure 4. Grazing-incidence X-ray diffraction (GIXD) of IDTBT film under strain. a) GIXD experiments set-up schematic with X-ray beam in different direction relative to stretched IDTBT films. The polymer backbones take face-on arrangement relative to substrate. b) 2D diffraction patterns of pristine IDTBT and DPPTT film (0% strain). GIXD diffractogram of 50% stretched IDTBT film. With the incidence light parallel (left) and perpendicular (right) to strain direction. c) The normalized crystallinity ratio ($R = I_{\parallel}/I_{\perp}$) at certain strain value for backbone (001) and π–π (010) diffraction peaks. (d) The normalized crystallinity with the incidence light at different angles relative to stretching direction for IDTBT films stretched at 0%, 50%, and 100% strain (when $\theta = 0$, the incidence light is parallel to strain direction). All of the calculated crystallinity were scaled for exposure time and illuminated volume.

The 2D pattern of IDTBT films at a certain strain was obtained with the incidence beam set to be parallel or perpendicular to strain direction (Figure S5, Supporting Information). For the spin-coated isotropic film, the (001) peak was present regardless of sample rotation relative to the beam direction. However, for a stretched film, polymer chain alignment induced by strain resulted in an increase in peak intensity parallel to the strain direction, as compared to the peak intensity perpendicular to the strain direction.[67] We employed these two principles in our analysis of the molecular chain alignment of IDTBT thin films under strain. 2D diffraction images of IDTBT thin film at 50% strain with the scattering factor q parallel and perpendicular to stretching direction are shown in Figure 4b. The (001) backbone diffraction peak has a higher intensity along the strain direction, qualitatively confirming anisotropic polymer chain alignment of IDTBT under strain. The detailed information on change in crystallinity for stretched IDTBT films can be found in Figure S6 (Supporting Information).

The extent of alignment of crystalline regions for IDTBT films under strain may be extracted by calculating the relative degree of crystallinity (rDOC). The normalized crystallinity ratio is defined as the ratio of peak intensity between the parallel and perpendicular direction ($R = I_{\parallel}/I_{\perp}$). The trend for the normalized crystallinity ratio change with strain was observed to be quite different for (010) and (001) peaks (Figure 4c). For the (010) peak, the ratio remained close to 1; thus, the out-of-plane π-π stacking was deemed not to be disrupted by strain. For the (001) peak, the ratio increased by three times at 50% strain compared with 0% strain; thus, there was more backbone ordering in the direction parallel to the strain compared to that in the perpendicular direction. This may be attributed to the reorientation of the small crystalline domains and polymer backbone alignment induced by strain. The calculated crystallographic parameters of the (001) backbone diffraction peak for the stretched IDTBT films showed negligible change in crystalline domain size under strain (Table S1, Supporting Information). The 2D GIXD patterns and detailed crystallinity information for stretched DPPTT films can be found in Figures S7 and S8 (Supporting Information). The in-plane π–π stacking (010) peak and out-of-plane lamella stacking (200) peak were chosen to calculate the normalized crystallinity ratio R during stretching. For the out-of-plane diffraction peak, the ratio remained close to 1. For the in-plane diffraction peak, the ratio also increased (Figure S8c, Supporting Information). However, when we compare the ratio change for the in-plane diffraction peak of DPPTT and IDTBT during stretching (Figure S8d, Supporting Information), we could see the alignment extent was weaker for DPPTT compared with IDTBT below 50% strain, which was due to crack formation. After 50% strain, the cracks propagated rapidly for DPPTT film, resulting in significant decrease of peak intensity

perpendicular to strain direction, thus R increased significantly from 50% to 75% strain.

To further confirm this morphology anisotropy during stretching, we conducted a rotation GIXD experiment.[68] We started with the sample placed along strain direction, and set θ as 0, then we rotated the sample by 180°, and calculated the rDOC at every 15° angle (Figure 4a). The normalized crystallinity (relative to the crystallinity at $\theta = 0$) at different angles at 0%, 50%, and 100% strain are shown in Figure 4d. At 0% strain (i.e., nonstretched), the crystalline domains had no preferential orientation. Once a strain was applied (e.g., at 50 or 100% strain), interestingly, the films showed much higher crystallinity with the incident X-ray parallel (i.e., 0 and 180°) to strain direction, and the crystallinity gradually decreased when the sample was rotated, and reached the lowest point as the X-ray placed perpendicularly (i.e., 90°) to strain direction. This observed trend confirmed our previous conclusion that the small crystallites exhibit preferential alignment along the stretching direction. At 100% strain, the rDOC anisotropy was more significant than 50% strain. Overall, these optical spectroscopic characterization methods confirmed that IDTBT polymer chains were well aligned during stretching in both crystalline and amorphous regions.

2.3. Electrical Characterizations

Transfer printing of stretched thin films has been widely employed to test the stretchability of semiconducting polymers.[29,45] Although devices for each strain must be individually fabricated, the transfer printing method largely excluded parameters that changes during stretching, such as the dielectric thickness and channel dimension. In this method, the thin film was transferred to a PDMS elastomer, stretched, then transferred to an azide-cross-linked SEBS dielectric, followed by deposition of Au electrodes (Figure S9, Supporting Information). Observations under brightfield microscopy and atomic force microscopy (AFM) also did not show any visible cracks formation (Figures S10 and S11, Supporting Information). The average mobility (Tables S2 and S3, Supporting Information) for IDTBT was observed to remain stable until 100% strain for a single loading in both the parallel and perpendicular direction relative to strain (**Figure 5**b), while the transfer curves for IDTBT-based OFET at different strain can be found in Figure S12 (Supporting Information). This was in stark contrast to the DPPTT film, in which the average mobility for DPPTT film decreased rapidly during stretching: decreasing three orders of magnitude parallel to strain direction and decreasing two orders of magnitude perpendicular to strain direction,[34] where the DPPTT films were transferred to monolayer modified SiO_2, such as *n*-octadecyltrimethoxysilane (OTMS) or benzocylobutene (BCB). One key parameter was the dielectric and its importance in this comparative study between IDTBT and DPPTT device characteristics upon stretching. For IDTBT, we found that nonideal device characteristics (i.e., the square root drain current was nonlinear at high gate voltage) were observed when monolayer -modified SiO_2 (OTS or BCB) was used as the dielectric, rendering an ambiguous extracted mobility. Conversely, the transfer curves with SEBS as the dielectric were close to ideal (Figure S13, Supporting Information). Moreover, most previously reported transport studies of IDTBT used CYTOP as the dielectric[40] and showed near-ideal and excellent performance. Thus, we speculated that nonpolar polymer dielectrics were desirable for IDTBT-based transistors. However, we observed the completely opposite phenomenon for DPPTT. We observed nonideal device characteristics when SEBS was used as the dielectric in bottom gate top contact device configuration, while the transfer curves were ideal when transferred onto monolayer-modified SiO_2. An important consideration when using the transfer printing method is the selection of an appropriate dielectric for both IDTBT and DPPTT. However, we found that the fully stretchable FETs with IDTBT or DPPTT as semiconductor showed ideal transfer characteristics, in which the extracted mobility value is reliable. Thus, in our comparative study, we focused on fabricating fully stretchable FETs (rather than the transfer printing method) to comparatively evaluate the charge transport properties of IDTBT and DPPTT polymer semiconductors under strain.

Fully stretchable organic transistors were fabricated and subjected to both a single loading and cyclic loading to evaluate the charge transport properties of the polymer films under strain. Our device architecture was bottom-gate top-contact, with PDMS as the stretchable dielectric and substrate, and conductive carbon nanotubes (CNTs) as the source, drain and gate electrodes (Figure 5a and Figure S14, Supporting Information). Importantly, a PDMS-based elastomer[69] was used to embed the CNT network gate to prevent damages to the dielectric layer upon stretching. Without strain, the device showed ideal transfer characteristics with low hysteresis, with and a high mobility ≈1.8 $cm^2\ V^{-1}\ s^{-1}$ and an on/off ratio of 10^6 (Figure 5c). To the best of our knowledge, this is the *highest* mobility reported for a fully stretchable organic device to date. Due to its rigid and coplanar backbone configuration, there are less traps in this polymer system, even reaching "disorder-free" limits as previously reported,[40] and intrachain charge transport was largely increased, resulting in high charge carrier mobility.

Fully stretchable IDTBT-based transistors displayed little degradation in performance at different strains during a single loading, as evidenced by the transfer curves (Figure 5f). Remarkably, the charge carrier mobility remained stable at ≈0.6 $cm^2\ V^{-1}\ s^{-1}$ at 100% strain along the strain direction. The decrease of the on-current due to the channel dimension and dielectric thickness change is expected to be 0.5 times, which is 0.25 times with observed decrease. In contrast, for a fully stretchable DPPTT-based transistor, the mobility decreased from 0.4 $cm^2\ V^{-1}\ s^{-1}$ at 0% strain to around 5×10^{-4} $cm^2\ V^{-1}\ s^{-1}$ at 100% strain along the strain direction (Figure 5e and Figure S15, Supporting Information). This observation again confirms that IDTBT can maintain sufficiently good electrical properties under mechanical strain due to its near-amorphous microstructure, compared with DPPTT with semicrystalline microstructure. The coplanar and rigid backbone configuration of IDTBT makes the charge transport mainly occur along conjugated backbones, while only requires occasional hopping across interchain π-π stacking. During stretching, IDTBT polymer chains slide past each other and dissipate strain energy, while the charge transport pathway is still maintained along conjugated backbones. For devices with active channels

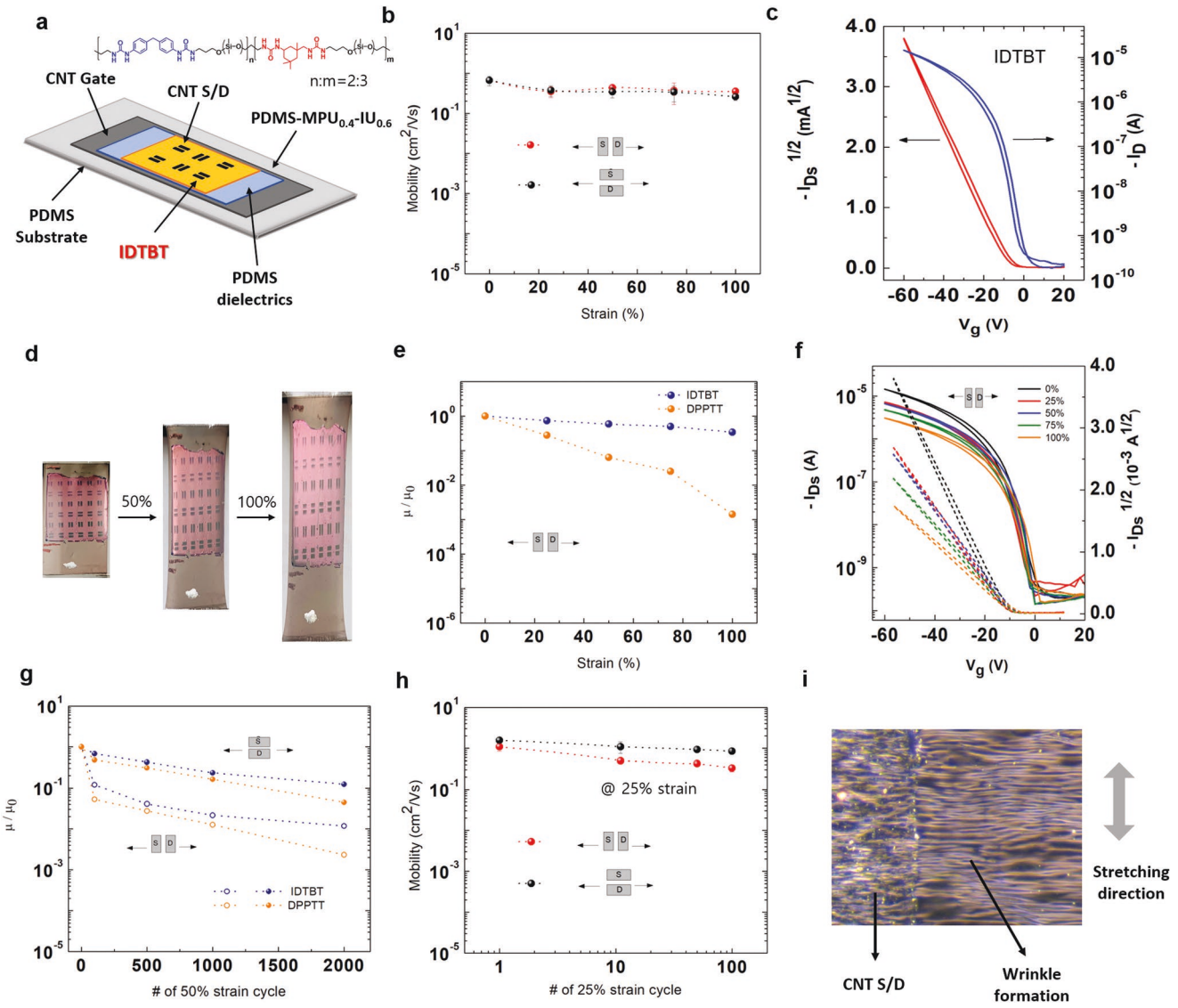

Figure 5. Electrical characterization of polymer thin films under strain. a) Bottom-gate top-contact device structure for fully stretchable organic transistors. b) Average mobility of stretched IDTBT films via the transfer-printing method, with azide-cross-linked SEBS as dielectric and Au as electrode. c) Transfer curve of a fully stretchable transistor with IDTBT as the semiconductor. Channel length L (150 μm), width W (1000 μm). The calculated dielectric capacitance is 8.85×10^{-6} F m^{-2}. d) Photograph of IDTBT fully stretchable transistor at 0%, 50%, 100% strain. e) Averaged normalized mobility of stretched polymer thin films in fully stretchable device configuration, with charge transport parallel to strain direction. f) Transfer curves of an IDTBT fully stretchable device under various strains, with the charge transport parallel to stretching direction. g) Average normalized mobility of IDTBT and DPPTT fully stretchable transistors at 50% strain over 2000 cycles. h) Average mobility of IDTBT fully stretchable transistors at 25% strain over 100 cycles. i) Optical microscope image of IDTBT film after 100 cycles at 50% strain. The mobility was extracted after channel dimension and dielectric capacitance correction.

in the direction perpendicular to strain, the average mobility decreased relatively more upon strain (Figure S16a, Supporting Information). At 100% strain, mobilities decreased from 1.8 to 0.1 cm^2 V^{-1} s^{-1} for IDTBT and from 0.4 to 1×10^{-5} cm^2 V^{-1} s^{-1} for DPPTT. Whereas the DPPTT mobility significantly decreased by four orders of magnitude upon strain due to crack propagation, the IDTBT mobility showed a minor decrease which may be due to more polymer chains were aligned along stretching direction, thus intrachain charge transport occurs more along strain rather than perpendicular to strain. In both parallel and perpendicular directions to strain, IDTBT had a much higher mobility than DPPTT. When we relaxed the IDTBT-based fully stretchable transistor from 100% strain, the charge transport decreased more parallel to strain direction (Figure S16c, Supporting Information) than the perpendicular direction, which was due to in-plane wrinkle formation (Figure 2e).

For practical applications, the device must reliably operate beyond a single loading cycling. Thus, we next evaluated the device performance of fully stretchable transistors over multiple stretching cycles. For both IDTBT and DPPTT, the mobility decreased correspondingly with increasing number of cycles at

50% strain (Figure 5g and Figure S17, Supporting Information). However, we note that these device performance degradation mechanisms were different. For IDTBT, plastic deformation at 50% strain was the main cause, as wrinkles were observed by optical microscopy after strain release (Figure 5i). For DPPTT, crack formation at 50% strain was the main cause. Distinct to the single loading results, the mobility for IDTBT was higher in the direction perpendicular to strain compared to the direction parallel to strain. This was due to the formation of in-plane wrinkling, where more chains were aligned perpendicular to strain direction when the film was relaxed.[70] The plastic deformation for IDTBT mode further supported the claim that IDTBT polymer chains can slide past each other due to large free volume and, thus, effectively dissipate strain energy. Since typical applied strain range from 20–30% for wearable applications,[7] we further tested the cyclic durability of IDTBT film at 25% strain. The device performance remained relatively stable until 100 cycles (Figure 5h and Figure S18, Supporting Information). However, in-plane wrinkling still formed at 25% strain (Figure S19, Supporting Information). These results indicated that the near-amorphous microstructures of IDTBT enabled its better stretchability under a single loading compared with semicrystalline conjugated polymer like DPPTT. Instead of crack formation, wrinkle formation was the major contributor to decreased device performance over cyclic loading due to plastic deformation and its low yield strain value. While IDTBT is highly ductile and can maintain sufficiently good charge transport properties under single mechanical loading, it undergoes plastic deformation which leads to poor cyclability. Further efforts need to put to impart higher elasticity in this polymer system.

3. Conclusion

In summary, we have successfully demonstrated that the near-amorphous polymer IDTBT is a promising candidate for intrinsically stretchable electronics applications. Despite its low crystallinity, IDTBT exhibited excellent charge transport properties. Compared to the semicrystalline DPPTT, IDTBT films showed improved plastic deformation due to the large free volume of polymer chains, and it can also help dissipate strain energy, as no crack propagation was observed until an applied 100% strain. From a morphology perspective, IDTBT polymer chains were observed to be much better aligned during stretching, both in crystalline and amorphous regions. Upon fabricating fully stretchable organic transistors with both IDTBT or DPPTT as active layer, we observed IDTBT-based devices had better performance under single loading and cyclic loading. This work represents the first study to show the usefulness of low crystallinity microstructures of polymer semiconductor to stable device performances under strain. Our results underscored the following molecular design guidelines toward achieving intrinsically stretchable high-performance polymer semiconductor, which are: i) low crystallinity could be achieved with long, bulky side chain attached on a tetrahedral carbon along polymer backbone, which may interrupt π–π stacking and reduce degree of crystallinity, and ii) rigid backbone configuration is desirable to minimize energetic disorder, thus facilitating more efficient intrachain charge transport. These understanding will further improvement of next-generation low crystallinity polymer system to possess both higher charge carrier mobility and stretchability.

4. Experimental Section

Thin Film Preparation: The polymer semiconductor solutions (10 mg mL^{-1} for IDTBT and 5 mg mL^{-1} for DPPTT) were prepared by dissolving the conjugated polymers in anhydrous chlorobenzene and stir overnight. Right before spin-coating, the polymer solutions were heated to 85 °C for 30 min. For the fabrication of these films, the polymer solutions were spun-cast on the highly doped n-type Si(100) wafers with 300 nm thick thermal SiO_2 modified with OTMS self-assembled monolayer following the reported method.[71] The IDTBT polymer thin film was prepared by spin-coating at 2000 rpm for 1 min, while the DPPTT polymer thin film was prepared by spin-coating at 1500 rpm for 1 min and then annealed at 150 °C for 30 min in nitrogen atmosphere.

Mechanical Characterizations: Film-on-Water Technique: The stress–strain curves were obtained from polymer thin films through pseudo-free-standing tensile test. The polymer thin films (≈50 nm) were first patterned into dog-bone shape according to previous report,[48] followed by floating transfer onto the top of water. Later, polymer films were unidirectionally pulled at a strain rate of 5×10^{-4} s^{-1} until the film fractures. At least six independent samples were measured for each conjugated polymer to provide statistically averaged mechanical properties. The elastic modulus was obtained from the slope of the linear fit of the stress–strain curve using the first 0.5% strain (elastic region).

Mechanical Characterizations: Nanoindentation Test: The elastic modulus was measured using dynamic displacement nanoindentation (Nanomechanics, Inc. iNano, Oak Ridge, TN) at a constant strain rate of 0.2% s^{-1} and a frequency of 160 Hz. During a nanoindentation test, a Berkovich tip was compressed into the sample while measuring the force and displacement. The Oliver-Pharr method was used to determine the elastic modulus and a Poisson's ratio of 0.3 was used for all calculations. Substrate effects were corrected for using the Hay-Crawford model. For compliant films on stiff substrates, the model was able to correct for the substrate effects up to 40% depth into the total film thickness. Samples were made by spin-coating DPPTT and IDTBT polymer onto a bare silicon wafer. An array of 16 indents was made on each polymer and the reported elastic modulus was the average of the moduli in the range of 20–30% depth into the total film thickness. The total thickness of the DPPTT specimen was determined using the profilometry to be 110 nm and IDTBT 81 nm. Data below 15 nm of depth, i.e., below 19% of total film thickness for IDTBT and below 14% for DPPTT, are not shown because of the noise resulted from the first contact made between the indenter tip and the specimen. The elastic modulus of DPPTT was 1.12 ± 0.19 GPa and IDTBT 2.46 ± 0.47 GPa.

The crack-on-set strain was measured by transferring thin films of polymer semiconductor onto PDMS (Sylgard 184, Dow Corning, precursor to cross-linker of 20:1, cured at 70 °C overnight, 1.2 mm in thickness). Then the polymer films on PDMS were stretched using a stretching station and the crack-on-set strain was monitored by optical microscope (Leica DM4000 M LED) from 0% strain to 100% strain. DMA was performed on a TA Instrument Q800 with a static force of 0.01 N, an oscillation strain of 0.1% at 1.0 Hz and a ramp rate of 2 °C min^{-1}. The polymer solutions were drop-casted on a polyimide substrate (thickness: 0.01 mm), and then the polymer thin films on polyimide substrate were loaded between the tension clamps of TA Instrument.

Morphological Characterizations: UV–vis absorption spectra were recorded on an Agilent Cary 6000i UV–Vis–NIR. For dichroic ratio measurement, polymer films were transferred onto PDMS (Sylgard 184, Dow Corning, precursor to cross-linker of 20:1, cured at 70 °C overnight, 1.2 mm in thickness) and stretched to certain strains, the absorption spectra were recorded with the polarized light parallel and

perpendicular to strain direction. The dichroic ratio for polymer films at different strain was also normalized by film thickness. The surface morphology of polymer thin film was obtained with a Nanoscope 3D controller AFM (Digital Instruments) operated in the tapping mode at room temperature. GIXD was performed at the Stanford Synchrotron Radiation Lightsource (SSRL) on beamline 11–3 and 7–2. The X-ray energy was 12.73 keV, and the incidence angle was 0.12°. Samples were measured in a helium chamber, and data analysis was performed in WxDiff.

Electrical Characterizations: Transfer Printing Method: Polymer semiconductor films on OTMS-treated SiO_2 substrates were transferred to a PDMS substrate (Sylgard 184, base/cross-linker, 12:1), stretched to the desired strain with a mechanical stretcher then slowly laminated on 1) highly doped n-type Si(100) substrate with dielectric layer as 300 nm thick thermal SiO_2 modified with monolayer, such as OTMS or BCB. 2) highly doped n-type Si (100) substrate with dielectric layer as azide-cross-linked SEBS. Then the PDMS substrate was gently lift up, leaving the strained semiconductor film on the dielectric layer. Top-contact gold electrodes (40 nm) in both parallel and perpendicular to strain direction were subsequently deposited by thermal evaporation through a shadow mask with channel length (L) and width (W) defined as 50 and 1000 µm, respectively. Azide-cross-linked SEBS[72] was used as dielectric layer to test the stretchability of IDTBT. The reason why we use this dielectric layer is that the near-amorphous IDTBT is relatively much softer than other semicrystalline conjugated polymer, which makes it hard to be transferred onto SiO_2 substrate with hydrophobic monolayer from PDMS. As SEBS is sticky, it could have good contact with IDTBT, thus we could obtain transferred strained IDTBT films with good quality. Bottom-gate top-contact devices were obtained, and the transistors were measured using a Keithley 4200 semiconductor parameter analyzer (Keithley Instruments Inc., Cleveland, OH, USA) under ambient atmosphere at room temperature.

Electrical Characterizations: Fully Stretchable OFET Fabrication: The semiconducting layer was prepared by spin coating polymer solution (10 mg mL^{-1} in chlorobenzene for IDTBT and 5 mg mL^{-1} for DPPTT) onto OTMS-treated Si wafer at 2000 rpm for 1 min for IDTBT, and 1500 rpm for 1 min for DPPTT. The resultant thickness for semiconducting layer was 40 nm. The solution for dielectric layer was prepared by diluting 5 g PDMS (Sylgard 184 [10:1] base vs cross linker) into 20 mL hexane. The dielectric layer was prepared by directly spin coating onto the semiconducting layer at 5000 rpm for 2 min. Then the substrate with the two layers was annealed in glove box at 80 °C for 2 h and 150 °C for 30 min. The temperature sequence is to make sure the PDMS dielectric layer is fully cross-linked and the polymer semiconductor is annealed at the same time to achieve better device performance. The resultant thickness for dielectric layer is around 2.4 µm as confirmed by Profilometer. Carbon nanotube (CNT) solution for gate was prepared by dispersing P2-SWNT with P3HT into chloroform (14 mg P2-SWNT / 4 mg P3HT/ 60 mL chloroform) through ultrasonication for 30 min at 30% amplitude using a 750 W ultrasonication probe, followed by centrifugation at 8000 rpm for 30 min. Then the gate layer was prepared by spray-coating CNT solution onto OTS treated Si wafer using a commercial airbrush (Master Airbrush, Model SB844-SET). PDMS-based tough elastomer[69] (PDMS-$MPU_{0.4}$-$IU_{0.6}$) solution (30 mg mL^{-1} in chloroform) was spin-coated onto the gate layer at 3000 rpm for 1 min to embed CNT network. The stretchable substrate was prepared by directly spin coating PDMS (Sylgard 184 [12:1] base vs cross linker) at 500 rpm for 30 s onto the embedding layer. Then the wafer was annealed at 70 °C overnight to fully cross-link PDMS elastomer substrate. The resultant thickness for substrate is around 1 mm. The gate layer was used to transfer the dielectric layer and semiconducting layer. Then we have the device structure from bottom to top as PDMS substrate, embedding layer, CNT gate, PDMS dielectric and polymer semiconductor. Finally, the source/drain electrodes were patterned by spray-coating dispersed P3-SWNT solution (6 mg/ 20 mL isopropanol) onto semiconducting layer through a shadow mask (L = 150 µm, W = 1000 µm). The stretchable OFET device structure is in bottom-gate top-contact configuration.

Supporting Information

Supporting Information is available from the Wiley Online Library or from the author.

Acknowledgements

This work was supported by Air Force Office of Scientific Research (Grant No. FA9550-18-1-0143) for financial support. M.N. acknowledges financial support from the European Commission through a Marie-Curie Individual Fellowship (EC Grant Agreement Number: 747461). H.T. was supported by an appointment to the Intelligence Community Postdoctoral Research Fellowship Program at Stanford University, administered by Oak Ridge Institute for Science and Education through an interagency agreement between the U.S. Department of Energy and the Office of the Director of National Intelligence. S.Z. and X.G. thank the financial support from U.S. Department of Energy, Office of Science, Office of Basic Energy Science under award number DE-SC0019361 and National Science Foundation Office of Integrative Activities #1757220. J.M. acknowledges Samsung Scholarship for financial support. Part of this work was performed at the Stanford Nano Shared Facilities (SNSF), supported by the National Science Foundation under award ECCS-1542152. GIXD measurement was carried out at the Stanford Synchrotron Radiation Laboratory (SSRL), a national user facility operated by Stanford University on behalf of the U.S. Department of Energy, Office of Basic Energy Sciences.

Conflict of Interest

The authors declare no conflict of interest.

Keywords

low crystallinity, polymer semiconductors, stretchable electronics

Received: July 3, 2019
Revised: August 14, 2019
Published online:

[1] A. Chortos, J. Liu, Z. Bao, *Nat. Mater.* **2016**, *15*, 937.
[2] Y. Liu, M. Pharr, G. A. Salvatore, *ACS Nano* **2017**, *11*, 9614.
[3] J. Rogers, G. Malliaras, T. Someya, *Sci. Adv.* **2018**, *4*, eaav1889.
[4] M. Caironi, C. Müller, E. von Hauff, M. Sommer, *Adv. Electron. Mater.* **2018**, *4*, 1800621.
[5] T. Someya, Z. Bao, G. G. Malliaras, *Nature* **2016**, *540*, 379.
[6] D. McCoul, W. Hu, M. Gao, V. Mehta, Q. Pei, *Adv. Electron. Mater.* **2016**, *2*, 1500407.
[7] N. Lu, D.-H. Kim, *Soft Rob.* **2014**, *1*, 53.
[8] S. Wang, J. Y. Oh, J. Xu, H. Tran, Z. Bao, *Acc. Chem. Res.* **2018**, *51*, 1033.
[9] Z. Bao, X. Chen, *Adv. Mater.* **2016**, *28*, 4177.
[10] D.-H. Kim, R. Ghaffari, N. Lu, J. A. Rogers, *Annu. Rev. Biomed. Eng.* **2012**, *14*, 113.
[11] J. A. Rogers, T. Someya, Y. Huang, *Science* **2010**, *327*, 1603.
[12] M. S. White, M. Kaltenbrunner, E. D. Głowacki, K. Gutnichenko, G. Kettlgruber, I. Graz, S. Aazou, C. Ulbricht, D. A. M. Egbe, M. C. Miron, Z. Major, M. C. Scharber, T. Sekitani, T. Someya, S. Bauer, N. S. Sariciftci, *Nat. Photonics* **2013**, *7*, 811.
[13] D.-H. Kim, J. Xiao, J. Song, Y. Huang, J. A. Rogers, *Adv. Mater.* **2010**, *22*, 2108.

[14] T. Someya, Y. Kato, T. Sekitani, S. Iba, Y. Noguchi, Y. Murase, H. Kawaguchi, T. Sakurai, *Proc. Natl. Acad. Sci. USA* **2005**, *102*, 12321.
[15] Y. Lee, M. Shin, K. Thiyagarajan, U. Jeong, *Macromolecules* **2016**, *49*, 433.
[16] J. E. Q. Quinsaat, M. Alexandru, F. A. Nüesch, H. Hofmann, A. Borgschulte, D. M. Opris, *J. Mater. Chem. A* **2015**, *3*, 14675.
[17] O. A. Araromi, S. Rosset, H. R. Shea, *ACS Appl. Mater. Interfaces* **2015**, *7*, 18046.
[18] S. P. Lacour, S. Wagner, Z. Huang, Z. Suo, *Appl. Phys. Lett.* **2003**, *82*, 2404.
[19] Y. Wang, C. Zhu, R. Pfattner, H. Yan, L. Jin, S. Chen, F. Molina-Lopez, F. Lissel, J. Liu, N. I. Rabiah, Z. Chen, J. W. Chung, C. Linder, M. F. Toney, B. Murmann, Z. Bao, *Sci. Adv.* **2017**, *3*, e1602076.
[20] S. Yao, Y. Zhu, *Adv. Mater.* **2015**, *27*, 1480.
[21] M. Vosgueritchian, D. J. Lipomi, Z. Bao, *Adv. Funct. Mater.* **2012**, *22*, 421.
[22] A. D. Printz, D. J. Lipomi, *Appl. Phys. Rev.* **2016**, *3*, 021302.
[23] G. J. N. Wang, A. Gasperini, Z. Bao, *Adv. Electron. Mater.* **2018**, *4*, 1700429.
[24] S. Savagatrup, X. Zhao, E. Chan, J. Mei, D. J. Lipomi, **2016**, *37*, 1623.
[25] Y. Zhao, X. Zhao, M. Roders, G. Qu, Y. Diao, A. L. Ayzner, J. Mei, *Chem. Mater.* **2015**, *27*, 7164.
[26] J. Mei, Z. Bao, *Chem. Mater.* **2014**, *26*, 604.
[27] X. Zhao, G. Xue, G. Qu, V. Singhania, Y. Zhao, K. Butrouna, A. Gumyusenge, Y. Diao, K. R. Graham, H. Li, J. Mei, *Macromolecules* **2017**, *50*, 6202.
[28] J. Mun, G.-J. N. Wang, J. Y. Oh, T. Katsumata, F. L. Lee, J. Kang, H.-C. Wu, F. Lissel, S. Rondeau-Gagné, J. B.-H. Tok, Z. Bao, *Adv. Funct. Mater.* **2018**, *28*, 1804222.
[29] H.-F. Wen, H.-C. Wu, J. Aimi, C.-C. Hung, Y.-C. Chiang, C.-C. Kuo, W.-C. Chen, *Macromolecules* **2017**, *50*, 4982.
[30] S. Zhang, M. U. Ocheje, L. Huang, L. Galuska, Z. Cao, S. Luo, Y. Cheng, D. Ehlenberg, R. B. Goodman, D. Zhou, Y. Liu, Y. Chiu, J. D. Azoulay, S. Rondeau-Gagné, X. Gu, *Adv. Electron. Mater.* **2019**, *5*, 1800899.
[31] J.-S. Kim, J.-H. Kim, W. Lee, H. Yu, H. J. Kim, I. Song, M. Shin, J. H. Oh, U. Jeong, T.-S. Kim, B. J. Kim, *Macromolecules* **2015**, *48*, 4339.
[32] T. Lei, J.-Y. Wang, J. Pei, *Acc. Chem. Res.* **2014**, *47*, 1117.
[33] G.-J. N. Wang, L. Shaw, J. Xu, T. Kurosawa, B. C. Schroeder, J. Y. Oh, S. J. Benight, Z. Bao, *Adv. Funct. Mater.* **2016**, *26*, 7254.
[34] J. Xu, S. Wang, G.-J. N. Wang, C. Zhu, S. Luo, L. Jin, X. Gu, S. Chen, V. R. Feig, J. W. F. To, S. Rondeau-Gagné, J. Park, B. C. Schroeder, C. Lu, J. Y. Oh, Y. Wang, Y.-H. Kim, H. Yan, R. Sinclair, D. Zhou, G. Xue, B. Murmann, C. Linder, W. Cai, J. B.-H. Tok, J. W. Chung, Z. Bao, *Science* **2017**, *355*, 59.
[35] R. Noriega, J. Rivnay, K. Vandewal, F. P. V Koch, N. Stingelin, P. Smith, M. F. Toney, A. Salleo, *Nat. Mater.* **2013**, *12*, 1038.
[36] Y. Yao, H. Dong, W. Hu, *Adv. Mater.* **2016**, *28*, 4513.
[37] S. Himmelberger, A. Salleo, *MRS Commun.* **2015**, *5*, 383.
[38] W. Zhang, J. Smith, S. E. Watkins, R. Gysel, M. Mcgehee, A. Salleo, J. Kirkpatrick, S. Ashraf, T. Anthopoulos, M. Heeney, I. McCulloch, *J. Am. Chem. Soc.* **2010**, *132*, 11437.
[39] H. Bronstein, D. S. Leem, R. Hamilton, P. Woebkenberg, S. King, W. Zhang, R. S. Ashraf, M. Heeney, T. D. Anthopoulos, J. De Mello, I. Mcculloch, *Macromolecules* **2011**, *44*, 6649.
[40] D. Venkateshvaran, M. Nikolka, A. Sadhanala, V. Lemaur, M. Zelazny, M. Kepa, M. Hurhangee, A. J. Kronemeijer, V. Pecunia, I. Nasrallah, I. Romanov, K. Broch, I. McCulloch, D. Emin, Y. Olivier, J. Cornil, D. Beljonne, H. Sirringhaus, *Nature* **2014**, *515*, 384.
[41] M. Nikolka, I. Nasrallah, B. Rose, M. K. Ravva, K. Broch, A. Sadhanala, D. Harkin, J. Charmet, M. Hurhangee, A. Brown, S. Illig, P. Too, J. Jongman, I. McCulloch, J. Bredas, H. Sirringhaus, *Nat. Mater.* **2017**, *16*, 356.
[42] X. Zhang, H. Bronstein, A. J. Kronemeijer, J. Smith, Y. Kim, R. J. Kline, L. J. Richter, T. D. Anthopoulos, H. Sirringhaus, K. Song, M. Heeney, W. Zhang, I. McCulloch, D. M. DeLongchamp, *Nat. Commun.* **2013**, *4*, 2238.
[43] Y. Li, W. K. Tatum, J. W. Onorato, Y. Zhang, C. K. Luscombe, *Macromolecules* **2018**, *51*, 6352.
[44] Y. Li, P. Sonar, L. Murphy, W. Hong, *Energy Environ. Sci.* **2013**, *6*, 1684.
[45] J. Y. Oh, S. Rondeau-Gagné, Y.-C. Chiu, A. Chortos, F. Lissel, G.-J. N. Wang, B. C. Schroeder, T. Kurosawa, J. Lopez, T. Katsumata, J. Xu, C. Zhu, X. Gu, W.-G. Bae, Y. Kim, L. Jin, J. W. Chung, J. B. H. Tok, Z. Bao, *Nature* **2016**, *539*, 411.
[46] S. Himmelberger, K. Vandewal, Z. Fei, M. Heeney, A. Salleo, *Macromolecules* **2014**, *47*, 7151.
[47] F. P. V. Koch, J. Rivnay, S. Foster, C. Müller, J. M. Downing, E. Buchaca-Domingo, P. Westacott, L. Yu, M. Yuan, M. Baklar, Z. Fei, C. Luscombe, M. A. McLachlan, M. Heeney, G. Rumbles, C. Silva, A. Salleo, J. Nelson, P. Smith, N. Stingelin, *Prog. Polym. Sci.* **2013**, *38*, 1978.
[48] S. Zhang, M. U. Ocheje, S. Luo, D. Ehlenberg, B. Appleby, D. Weller, D. Zhou, S. Rondeau-Gagné, X. Gu, *Macromol. Rapid Commun.* **2018**, *39*, 1800092.
[49] J.-H. Kim, A. Nizami, Y. Hwangbo, B. Jang, H.-J. Lee, C.-S. Woo, S. Hyun, T.-S. Kim, *Nat. Commun.* **2013**, *4*, 2520.
[50] C. Lu, W.-Y. Lee, X. Gu, J. Xu, H.-H. Chou, H. Yan, Y.-C. Chiu, M. He, J. R. Matthews, W. Niu, J. B. H. Tok, M. F. Toney, W.-C. Chen, Z. Bao, *Adv. Electron. Mater.* **2017**, *3*, 1600311.
[51] S. Savagatrup, A. S. Makaram, D. J. Burke, D. J. Lipomi, *Adv. Funct. Mater.* **2014**, *24*, 1169.
[52] J. Onorato, V. Pakhnyuk, C. K. Luscombe, *Polym. J.* **2017**, *49*, 41.
[53] I. McCulloch, R. S. Ashraf, L. Biniek, H. Bronstein, C. Combe, J. E. Donaghey, D. I. James, C. B. Nielsen, B. C. Schroeder, W. Zhang, *Acc. Chem. Res.* **2012**, *45*, 714.
[54] A. V. Tobolsky, *J. Appl. Phys.* **1956**, *27*, 673.
[55] N. Balar, B. T. O'Connor, *Macromolecules* **2017**, *50*, 8611.
[56] X. Li, J. Liu, Z. Liu, M. Tsige, S. Q. Wang, *Phys. Rev. Lett.* **2018**, *120*, 77801.
[57] Z. Qian, Z. Cao, L. Galuska, S. Zhang, J. Xu, X. Gu, *Macromol. Chem. Phys.* **2019**, *220*, 1900062.
[58] G. J. N. Wang, F. Molina-Lopez, H. Zhang, J. Xu, H. C. Wu, J. Lopez, L. Shaw, J. Mun, Q. Zhang, S. Wang, A. Ehrlich, Z. Bao, *Macromolecules* **2018**, *51*, 4976.
[59] B. Roth, S. Savagatrup, N. V. de los Santos, O. Hagemann, J. E. Carlé, M. Helgesen, F. Livi, E. Bundgaard, R. R. Søndergaard, F. C. Krebs, D. J. Lipomi, *Chem. Mater.* **2016**, *28*, 2363.
[60] T. Lei, J.-H. Dou, J. Pei, *Adv. Mater.* **2012**, *24*, 6457.
[61] S. E. Root, S. Savagatrup, A. D. Printz, D. Rodriquez, D. J. Lipomi, *Chem. Rev.* **2017**, *117*, 6467.
[62] M. A. Alkhadra, S. E. Root, K. M. Hilby, D. Rodriquez, F. Sugiyama, D. J. Lipomi, *Chem. Mater.* **2017**, *29*, 10139.
[63] B. G. Kim, E. J. Jeong, J. W. Chung, S. Seo, B. Koo, J. Kim, *Nat. Mater.* **2013**, *12*, 659.
[64] J. Rivnay, S. C. B. Mannsfeld, C. E. Miller, A. Salleo, M. F. Toney, *Chem. Rev.* **2012**, *112*, 5488.
[65] H. R. Tseng, H. Phan, C. Luo, M. Wang, L. A. Perez, S. N. Patel, L. Ying, E. J. Kramer, T. Q. Nguyen, G. C. Bazan, A. J. Heeger, *Adv. Mater.* **2014**, *26*, 2993.
[66] J. Rivnay, M. F. Toney, Y. Zheng, I. V Kauvar, Z. Chen, V. Wagner, A. Facchetti, A. Salleo, *Adv. Mater.* **2010**, *22*, 4359.
[67] M. Wang, M. J. Ford, C. Zhou, M. Seifrid, T. Q. Nguyen, G. C. Bazan, *J. Am. Chem. Soc.* **2017**, *139*, 17624.
[68] F. Molina-Lopez, H. C. Wu, G. J. N. Wang, H. Yan, L. Shaw, J. Xu, M. F. Toney, Z. Bao, *Adv. Electron. Mater.* **2018**, *4*, 1800110.

[69] J. Kang, D. Son, G.-J. N. Wang, Y. Liu, J. Lopez, Y. Kim, J. Y. Oh, T. Katsumata, J. Mun, Y. Lee, L. Jin, J. B. H. Tok, Z. Bao, *Adv. Mater.* **2018**, *30*, 1706846.

[70] G.-J. N. Wang, Y. Zheng, S. Zhang, J. Kang, H.-C. Wu, A. Gasperini, H. Zhang, X. Gu, Z. Bao, *Chem. Mater.* **2018**, acs.chemmater.8b04314.

[71] Y. Ito, A. A. Virkar, S. Mannsfeld, J. H. Oh, M. Toney, J. Locklin, Z. Bao, *J. Am. Chem. Soc.* **2009**, *131*, 9396.

[72] S. Wang, J. Xu, W. Wang, G.-J. N. Wang, R. Rastak, F. Molina-Lopez, J. W. Chung, S. Niu, V. R. Feig, J. Lopez, T. Lei, S.-K. Kwon, Y. Kim, A. M. Foudeh, A. Ehrlich, A. Gasperini, Y. Yun, B. Murmann, J. B. H. Tok, Z. Bao, *Nature* **2018**, *555*, 83.